Effect of magnetic impurities on the vortex lattice properties in $NbSe_2$ single crystals

M. Iavarone,[1] R. Di Capua,[2,3] G. Karapetrov,[1] A. E. Koshelev,[1] D. Rosenmann,[1,*] H. Claus,[1] C. D. Malliakas,[1,4] M. G. Kanatzidis,[1,4] T. Nishizaki,[5] and N. Kobayashi[5]

[1]*Materials Science Division, Argonne National Laboratory, Argonne, Illinois 60439, USA*

[2]*Dipartimento S.pe.S., Università degli Studi del Molise, Via De Sanctis, I-86100 Campobasso, Italy*

[3]*CNR-INFM COHERENTIA, Complesso di Monte S. Angelo, Via Cinthia, I-80126 Napoli, Italy*

[4]*Department of Chemistry, Northwestern University, Evanston, Illinois 60208, USA*

[5]*Institute for Materials Research, Tohoku University, Sendai 980-8577, Japan*

(Received 1 August 2008; revised manuscript received 7 October 2008; published 17 November 2008)

We report a pronounced peak effect in the magnetization of Co_xNbSe_2 single crystals with critical temperatures T_c ranging between 7.1 and 5.0 K, and Mn_xNbSe_2 single crystals with critical temperatures down to 3.4 K. We correlate the peak effect in magnetization with the structure of the vortex lattice across the peak-effect region using scanning-tunneling microscopy. Magnetization measurements show that the amplitude of the peak effect in the case of Co_xNbSe_2 exhibits a nonmonotonic behavior as a function of the Co content, reaching a maximum for concentration of Co of about 0.4 at. % (corresponding to a T_c of 5.7 K) and after that gradually decreasing in amplitude with the increase in the Co content. The normalized value of the peak position H_p/H_{c2} has weak dependence on Co concentration. In the case of Mn_xNbSe_2 the features of the peak effect as a function of the Mn content are different and they can be understood in terms of strong pinning.

DOI: 10.1103/PhysRevB.78.174518 PACS number(s): 74.50.+r, 74.25.Jb, 74.70.Ad

I. INTRODUCTION

The understanding of the origin of finite critical current in type-II superconductors is a challenging problem. The competition between the elastic properties of the vortex lattice (VL) and the energy landscape defined by the pinning centers can stabilize different vortex matter states. In this respect, the peak effect, i.e., a sudden increase in the critical current density J_c close to the upper critical field H_{c2}, has been extensively studied for a long time and with many different experimental techniques.[1–5] The Larkin-Ovchinnikov collective-pinning model[6] provides the traditional theoretical framework for the origin of the peak effect as a softening of the VL and a crossover between collective and single-vortex pinnings. This theory links the enhanced critical current density near H_{c2} to the loss of long-range order in the otherwise periodic Abrikosov vortex lattice and the formation of the finite-size-ordered vortex lattice domains. Vortex lattice lines have been studied by Lorentz microscopy,[7] Bitter decoration,[8] and scanning superconducting quantum interference device (SQUID) microscopy.[9] The above techniques are sensitive to the spatial profile of the magnetic field and therefore they are effective at low applied magnetic fields at which the vortices are far away and the interaction between them is weak. Moreover, contradictory experimental results have been reported in literature. Indeed, Bitter-decoration experiments showed that no correlation between peak effect and the topology of the vortex structure can be made in the disordered phase of Fe-doped $NbSe_2$.[8] However, the measurements were performed at low fields and in this case the dislocations of the VL were observed mainly at the grain boundaries. The region of high magnetic fields has been investigated by neutron scattering[10] and, more recently, by scanning-tunneling microscopy (STM).[11] In the latter the transition from collective vortex motion to positional fluctuations of individual vortices in a sample of $NbSe_2$ has been associated to the peak effect observed in ac susceptibility.

In this paper we aim to correlate the behavior of the vortex matter in Co_xNbSe_2 and Mn_xNbSe_2 single crystals with the amounts of Co and Mn concentrations. By varying the concentrations of Co and Mn, we could tune the superconducting properties of the material and the pinning of the VL. We find that magnetic impurities provide efficient pinning for the VL through the local variation in critical temperature, i.e., δT_c-pinning. A pronounced peak effect in dc magnetization measurements is correlated with the structure of the VL by using low-temperature STM in magnetic fields corresponding to the peak-effect region. An interplay between anisotropy of the upper critical field and a collective weak pinning character of the pinning centers can explain some of the observed features of the peak effect as a function of the Co concentration. The features of the peak effect in Mn_xNbSe_2 are different and they could be attributed to the strong pinning induced by the large localized magnetic moment of Mn ions.

II. SAMPLES

Intercalation of atoms between the weakly coupled planes of Se atoms (i.e., van der Waals space) leads to significant modification of the physical properties of $NbSe_2$. A variety of magnetic and nonmagnetic atoms were reported to be intercalated in $NbSe_2$.[12] Cobalt- and manganese-intercalated $NbSe_2$ single crystals were grown starting from raw materials by iodine-vapor transport at 900 °C.[13] X-ray diffraction pattern showed that they have the same structure as 2H-$NbSe_2$. The Co and the Mn content was determined by energy-dispersive x-ray microprobe analysis (EDS). Multiple regions on each crystal surface were analyzed. The EDS spectrum showed that the atomic concentrations of Co and Mn at different locations of each crystal were similar, which, together with the sharp superconducting transition, indicates

TABLE I. Summary of the single crystals investigated. The concentrations of Co and Mn dopants were obtained by EDS. The critical temperatures T_c; the upper critical field for fields applied along the c axis of the crystals at 1.8 K, $H_{c2}^{\|}(1.8\ \mathrm{K})$; and the anisotropy of the upper critical field γ have been measured with dc SQUID magnetometry.

	Formula	Co, Mn (at. %)	T_c (K)	$\mu_0 H_{c2}^{\|}(1.8\ \mathrm{K})$ (T)	$\gamma=\left(\frac{(dH_{c2}/dT)_\perp}{(dH_{c2}/dT)_\|}\right)_{T=T_c}$
Pure $NbSe_2$	$NbSe_2$		7.1	3.6	3.2
Co1	$Co_{0.0045}NbSe_2$	0.15	6.6	3.2	3.1
Co2	$Co_{0.0075}NbSe_2$	0.25	6.3	3.4	2.55
Co3	$Co_{0.010}NbSe_2$	0.33	6.0	3.6	2.45
Co4	$Co_{0.012}NbSe_2$	0.40	5.7	3.4	2.37
Co5	$Co_{0.013}NbSe_2$	0.45	5.5	2.8	2.30
Co6	$Co_{0.016}NbSe_2$	0.55	5.0	2.4	2.57
Mn1	$Mn_{0.0012}NbSe_2$	0.04	5.8	2.38	3.15
Mn2	$Mn_{0.0045}NbSe_2$	0.15	3.4	0.85	3.15

that the crystals are homogeneous. The superconducting critical temperature was determined by SQUID magnetometry and measured in a small applied field ($H=1$ Oe). In this paper we investigate samples with a dilute concentration of Co and Mn. For these samples the reduction in T_c with increasing dopant content is linear at a rate of about 3 K/at. % of Co and at about 25 K/at. % of Mn, in agreement with earlier reports.[14,15] The width of the transition ΔT_c (10%–90% criterion) ranges between 0.1 K (for samples with T_c down to 5.7 K) and 0.25 K (for samples with T_c from 5.3 to 5.0 K) for the Co and less than 0.1 K in the case of Mn intercalation. Table I summarizes the Co and Mn contents of the crystals investigated, the superconducting critical temperatures, the upper critical fields at 1.8 K derived from magnetization isothermal loops for field applied parallel to the c axis ($H_{c2}^{\|}$), and the anisotropy of the upper critical field defined as the ratio of the slopes dH_{c2}/dT close to the critical temperature T_c for fields parallel and perpendicular to the crystallographic c axis of the samples, $\gamma=\left(\frac{(dH_{c2}/dT)_\perp}{(dH_{c2}/dT)_\|}\right)_{T=T_c}$.

III. MAGNETIZATION MEASUREMENTS

A. Normal-state magnetization

Temperature dependences of the magnetic susceptibilities, $\chi=M/H$, parallel and perpendicular to the layers of the first-row transition-metal intercalates of dichalcogenides have been widely studied in the past in the range of high intercalation concentration ($x=1/3$ and $x=1/4$). These metal intercalation complexes are particularly interesting because at high concentration the $3d$ ions form ordered superlattices which show ferromagnetic and antiferromagnetic orderings.[16] There is also evidence for charge transfer from the transition-metal ion to the Nb d-orbital band, resulting in oxidation state of (2+) or (3+) for the transition-metal ion. The remaining d electrons on the $3d$ intercalated ions are localized and show magnetic moments.

In the range of intercalation concentrations studied in this paper, we did not observe any magnetic ordering for either Co_xNbSe_2 or Mn_xNbSe_2 single crystals. The magnetic susceptibilities between 4.2 and 100 K for Co4, Mn1, and pure $NbSe_2$ single crystals with the applied magnetic field of 4 T parallel to the c axis are shown in Fig. 1. The susceptibility of pure $NbSe_2$ exhibits a large Pauli-paramagnetic component that is temperature dependent above 100 K and temperature independent below 100 K. The temperature dependence of the susceptibilities of the Co- and Mn-intercalated crystals shows a Curie-Weiss behavior, in agreement with previous findings:[16]

$$\chi=\chi_0+\frac{C}{T+\theta}=\chi_0+\frac{N\mu_{\mathrm{eff}}^2}{3k_B(T+\theta)}, \tag{1}$$

where C is the Curie constant from which an effective moment μ_{eff} can be derived, T is the temperature, θ is the Weiss constant, N is the number of magnetic atoms and χ_0 is the temperature-independent term. This term can be represented in the form $\chi_0=\chi_d+\chi_P$, where χ_d is the diamagnetism of the ion core and χ_P is the Pauli-paramagnetic contribution. The value of χ_d should be reasonably the same for different intercalated metal atoms, while the value of χ_P should depend upon the number of free electrons in the $4d$ band, and therefore it will depend upon the type of the dopant metal atom.

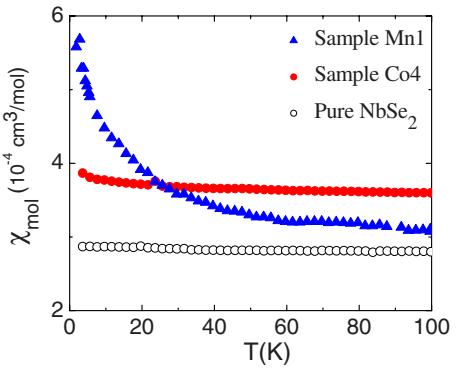

FIG. 1. (Color online) Magnetic susceptibilities of $NbSe_2$, Co_xNbSe_2 (sample Co4), and Mn_xNbSe_2 (sample Mn1) single crystals in a magnetic field $H=4$ T applied parallel to the c axis.

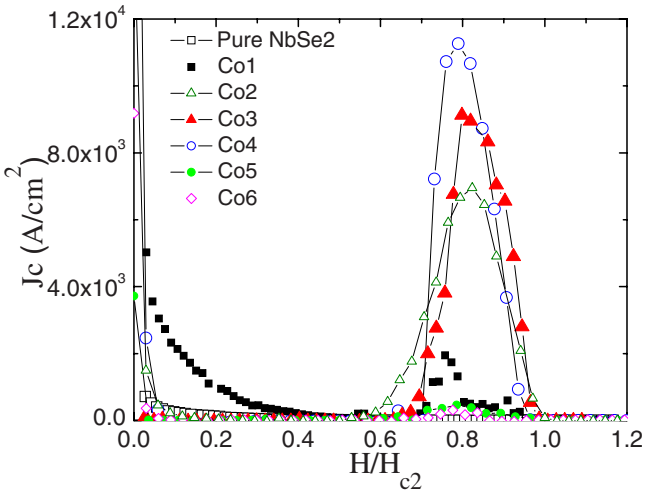

FIG. 2. (Color online) Critical current density obtained from the irreversibility of the isothermal magnetization curves for pure $NbSe_2$ and Co_xNbSe_2 single crystals with different T_c ranging from 7.1 to 5.0 K.

For both Co_xNbSe_2 and Mn_xNbSe_2 single crystals in the range of x explored, we observed that the temperature-independent term increased compared to pure $NbSe_2$, which implies an increase in the concentration of free electrons.

In order to obtain the Co and Mn moments in Co_xNbSe_2 and Mn_xNbSe_2, respectively, we used the temperature-dependent susceptibility data below 100 K. Above 100 K the temperature dependence of the susceptibility could arise from a large Pauli paramagnetism observed also in pure $NbSe_2$ crystals. For $Co_{0.012}NbSe_2$ we find $\mu_{\text{eff}}=0.6\mu_B$ per Co atom and $\theta=13$ K. For $Mn_{0.0012}NbSe_2$ we find $\mu_{\text{eff}}=4.2\mu_B$ per Mn atom and $\theta=7$ K. Therefore, both Co and Mn have a localized magnetic moment. In the case of Co we find that the small value of μ_{eff} obtained is only consistent with the low-spin $3d^7$-electron configuration of Co^{2+} $(S=1/2)$, in agreement with previous findings.[14] In the case of Mn the value of μ_{eff} is close to the spin-only moment $[\mu_{\text{eff}}=\sqrt{n(n+1)}\mu_B$, where n is the number of unpaired electrons] of Mn^{3+} in the high-spin $3d^4$-electron configuration $(S=2)$, consistent with data reported earlier in literature.[17]

B. Superconducting-state magnetization

dc magnetization measurements were performed with a SQUID magnetometer (Quantum Design). The magnetization hysteresis loops of the Co- and Mn-intercalated $NbSe_2$ single crystals were measured at different temperatures and in applied magnetic fields parallel and perpendicular to the crystallographic c axis of the single crystals. The critical current density J_c is directly proportional to the irreversible magnetization of the sample. It was obtained from the isothermal magnetization curves at 1.8 K in magnetic field H applied parallel to the c axis of the crystal structure. According to the Bean model,[18] $J_c \propto \Delta M/d$, where M is the magnetization of the sample, ΔM is the width of the magnetization hysteresis loop, and d is the thickness. In Fig. 2 the critical current density J_c is plotted as a function of the normalized field $h=H/H_{c2}^{\parallel}$, for samples with different concentrations of Co at the temperature of 1.8 K. The "pure $NbSe_2$" sample is a pristine single crystal used as a reference. The critical current density of this sample was about 700 A/cm^2 and no peak effect could be detected near the upper critical field within resolution in the isothermal magnetization curve down to 1.8 K. Sample Co1, with smallest Co content and therefore lower $T_c=6.6$ K, shows a similar irreversibility in magnetization, but a peak effect appears close to H_{c2}. An increase in the Co content (sample Co2) leads to a reversible magnetization in the wide range of fields below the peak-effect region. Concurrently, a strong enhancement of the peak-effect amplitude close to H_{c2} is observed, with maximum value of the current density reaching 10^4 A/cm^2. The peak-effect region is also characterized by an abrupt onset field. A comparable magnetization curve is observed for sample Co3 with $T_c=6.0$ K. Further increase in Co content leads to a gradual decrease in the amplitude of the peak effect while the magnetization continues to exhibit reversible behavior at low fields. The value of the maximum critical current density in the peak-effect regime, $J_{c\max}$, is therefore a nonmonotonic function of the Co content and consequently of the critical temperature of the sample. $J_{c\max}$ reaches its maximum value for an optimal Co content of 0.4 at. % (corresponding to a T_c of 5.7 K) and then slowly decreases as the Co content is increased, anticorrelating with the amount of disorder. The normalized value of the peak position, $\frac{H_{\text{peak}}}{H_{c2}}$, remains almost unchanged at different dopings and ranges between 0. 75 and 0.80 H_{c2}. The same behavior has been observed at 4.2 K except for the sample with the lowest $T_c=5.0$ K, in which no peak effect was observed at 4.2 K.

The main features of the $J_c(H)$ as a function of the Co concentration can be summarized as follows. *Firstly*, beyond a critical Co concentration the magnetization curve becomes reversible, within experimental resolution, at very low fields and the reversible magnetization region extends for most of the mixed state. This wide region of reversible magnetization indicates a very weak pinning, resulting in a near-zero critical current density. One might find surprising the fact that slight irreversibility present in the pure $NbSe_2$ sample and sample Co1 at low fields is reduced with the increase in Co content. Intuitively, the Co impurities should act as pinning centers for the VL.

Secondly, the J_c peak height is a nonmonotonic function of the Co concentration. Conventionally, the peak effect in $NbSe_2$ single crystals has been explained as a crossover from collective to single-vortex pinning. Transport measurements show that the pinning force depends on the pin density n as n^2 in fields below the peak effect (collective pinning) and as n in the peak-effect regime (single-vortex pinning).[19] This seems to be in contrast to our data.

Thirdly, the fact that the normalized peak position does not shift downward with n means that the order-disorder line does not shift away from the $H_{c2}(T)$ boundary. This is perhaps the most surprising feature and does not agree with the Larkin-Ovchinnikov picture of the peak effect.

Magnetization measurements of the Mn-intercalated crystals show distinctively different behavior of the peak effect from that of Co-doped $NbSe_2$. The peak-effect feature in the

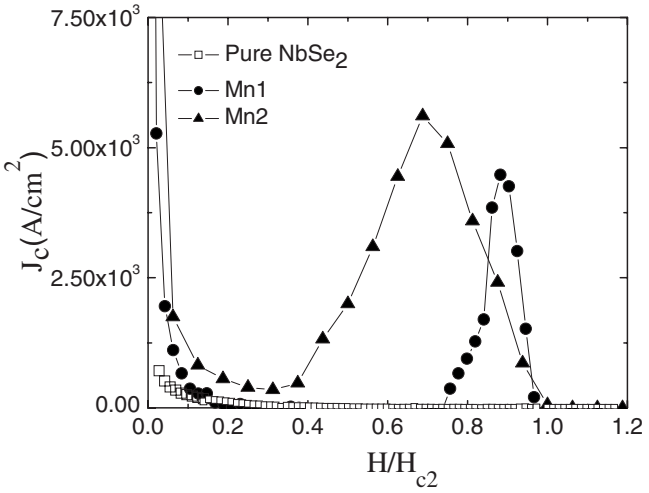

FIG. 3. Critical current density obtained from the irreversibility of the isothermal magnetization curves for pure $NbSe_2$ and Mn_xNbSe_2 single crystals with different T_c ranging from 7.1 to 3.4 K.

Mn_xNbSe_2 single crystals is summarized in Fig. 3. We obtain a similar magnitude of the peak effect in $J_c(H)$ with much smaller concentration of pinning centers since Mn suppresses the superconducting critical temperature T_c much more strongly. However, the three distinct features of the peak effect attributed to Co_xNbSe_2 are not observed in this case. The critical current density actually increases with doping concentration at low fields. Moreover, as the number of pinning centers increases, the order-disorder line shifts away from the $H_{c2}(T)$ boundary.

The upper critical fields parallel, $H_{c2}^{\parallel}$, and perpendicular, $H_{c2}^{\perp}$, to the c axis of the crystals were determined by the isothermal magnetization loops. The upper critical fields of $NbSe_2$ have been investigated by a number of researchers.[20–22] We find a linear behavior of H_{c2} vs T above 1.8 K and an anisotropy of $\gamma=3.2$ for the pure $NbSe_2$, in agreement with previous findings. As we increase the concentration of Co and Mn, the anisotropy of the upper critical field changes. It decreases in the case of Co-intercalated samples and it is almost constant for the Mn-intercalated crystals compared to the pure $NbSe_2$ case (see Table I). This difference in the anisotropy of the upper critical field γ with doping could explain the opposite tendency of the irreversible magnetization at low fields. Indeed, a reduction in the anisotropy of the upper critical field (in the case of Co doping) implies stiffer vortex lines for the case $H\|c$, which leads to an increased energy required to pin the lattice and consequently will decrease the critical current density. The effective tilt modulus c_{44} of the VL scales as γ^{-2}.[23] Therefore, as anisotropy γ decreases, the vortex lines are less "adaptable" to bending in order to accommodate to the point pinning centers of Co. Thus the J_c at low magnetic fields vanishes with Co doping. In the case of Mn the anisotropy is constant throughout the doping range studied. So the relative increase in the amount of pinning centers (by excess of 100% between Mn1 and Mn2 samples) enhances significantly the critical current at low fields, while anisotropy remains unchanged.

IV. IMAGING OF THE VORTEX LATTICE

The structural changes in the VL were investigated using low-temperature STM at 4.2 K as well as at 1.8 K and in magnetic fields corresponding to the regime of the peak effect. The STM allows us to visualize the VL at different magnetic fields applied parallel to the c axis of the sample by spatial mapping of the tunneling differential conductance (proportional to the electronic local density of states close to the Fermi level). In Fig. 4 a set of raw and processed STM data at 1.8 K and at five different magnetic fields are shown. The measurements have been performed in zero-field-cooled regime. After applying each magnetic field we waited for 30 min before performing STM imaging. Each image corresponds to a scanning area of 375×375 nm^2 and the scanning acquisition time was about 3 h, which allowed us to obtain high-quality images. The images were acquired at a voltage corresponding to the superconducting gap energy of the sample and at a tunneling current of about 10 pA. In Fig. 4 we show VL images obtained on sample Co4 at 1.8 K and at five magnetic fields: (a) 1.8 T, well below the onset of the peak-effect region in the isothermal magnetization curve shown in Fig. 5(a); (b) 2.3 T, corresponding to the onset of the peak-effect region; (c) 2.5 T, between the onset and the peak; (d) 2.7 T, at a field corresponding to H_{peak}; (e) 3.3 T, above H_{peak} and very close to H_{c2}. The first image [Fig. 4(a)] at 1.8 T shows a perfect vortex arrangement without visible distortions. At the onset of the peak-effect region [Fig. 4(b)], an almost perfect lattice is still observed with only a couple of defects. At the field of 2.5 T [Fig. 4(c)], an abrupt change in the structure of the lattice is observed that persists in higher fields [Figs. 4(d) and 4(e)]. Several image-processing procedures were used in order to extract orientational and positional orders in the vortex structure. For each image we calculated the autocorrelation and the pair-correlation functions. The autocorrelation function is defined as

$$G(\mathbf{r}) = \sum_{\mathbf{r}'} f(\mathbf{r}')f(\mathbf{r}'+\mathbf{r}),$$

where $f(\mathbf{r}')$ is the raw data image matrix. Each term in the sum multiplies the image and the same image shifted by a distance $\mathbf{r}$ with respect to the center of the image. The resulting image $G(\mathbf{r})$ is a measure of how different the two images are. The more similar the image and the shifted image are, the higher is the value of autocorrelation. Any periodicity in the original image will be shown as a periodic pattern in the autocorrelation image. It is worth noting that the autocorrelation function has been calculated from the raw STM images. Therefore in the region of high fields possible artifacts can be induced by the vortex shape.

The spatial order of the VL can be analyzed with the two-dimensional pair-correlation function, which is defined as the number of pairs with separation r per unit area. It represents the probability of finding a particle at a given distance from another:

$$g(r) = \sum_i \sum_j \frac{A}{2\pi r_{ij} N^2} d(r - r_{ij}),$$

where N is the total number of particles, A is the scanning area, r_{ij} is the distance between vortex j and vortex i, and the

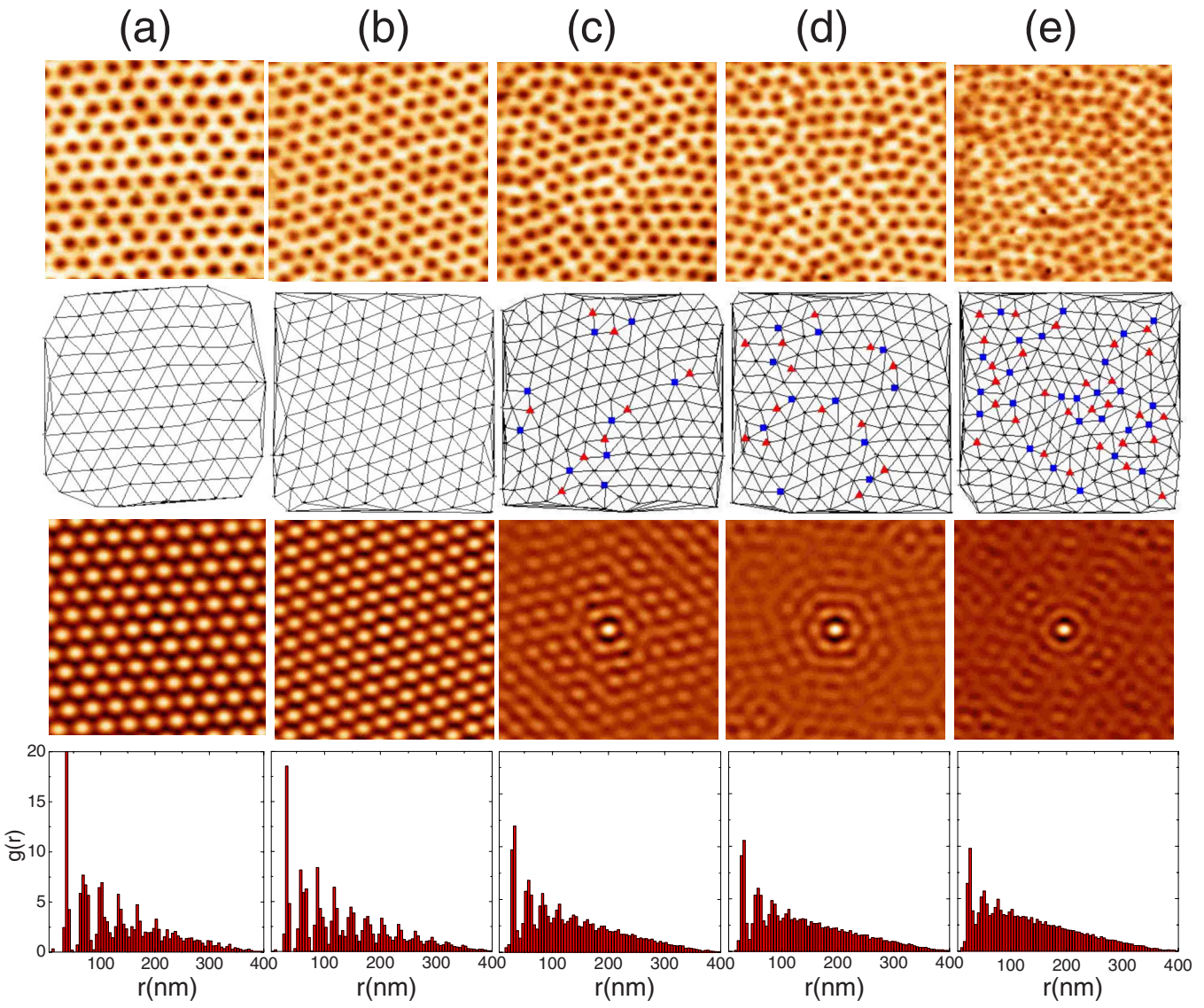

FIG. 4. (Color online) Raw and processed STM images from a sequence acquired at 1.8 K on sample Co4 at different magnetic fields applied perpendicular to the crystal surface. The first-row images represent the raw data of the conductance acquired at fields (a) $H=1.8$, (b) 2.3, (c) 2.5, (d) 2.7, and (e) 3.3 T. The second-row images represent the Delauney triangulation, with the triangles corresponding to defects with coordination number 5, while the squares correspond to defect with coordination number 7. The third image in the column is the autocorrelation of the STM image, and the fourth is the pair-correlation function obtained from the arrays of vortex coordinates derived from the STM image. The scanning area for all images is 375×375 nm^2.

sum runs over all the pairs of vortices in the image. For a perfect lattice the pair-correlation function will have peaks corresponding to the first-, second-, third-, etc., nearest neighbors. When the lattice starts to disorder, the pair-correlation function will show only few nearest-neighbor peaks and eventually for fully disordered lattice no peaks will be visible except the first one. Of course, this analysis will be limited by the number of vortices in the images and therefore, by the available scanning area and applied magnetic field. The second image in each column of Fig. 4 is the Delauney triangulation[24] of the vortex lattice, the third image in each column is the calculated autocorrelation from the STM image, while the fourth graph in each column of Fig. 4 is the pair-correlation function calculated from the vortex coordinates in each image. In Fig. 4(a) we show the Delauney triangulation, the autocorrelation, and the pair-correlation functions for a perfect lattice. In this case the autocorrelation reproduces the periodicity of the lattice and the pair-correlation function shows peaks up to the fourth-nearest neighbor. The same analysis for $H=2.3$ T [Fig. 4(b)] still shows quite an ordered vortex lattice and the pair-correlation function shows peaks up to the seventh-nearest neighbor, reflecting the fact that the number of vortices in the same scanning area increases with increasing magnetic field. At $H=2.5$ T, although the number of vortices in the image increased, the pair-correlation function [Fig. 4(c)] shows peaks corresponding only to the first-, second-, and third-nearest neighbors, i.e., ordered domains with sizes not bigger than $3a_0$, where a_0 is the distance between vortices at a given field. Although some periodicity is still present in the auto-

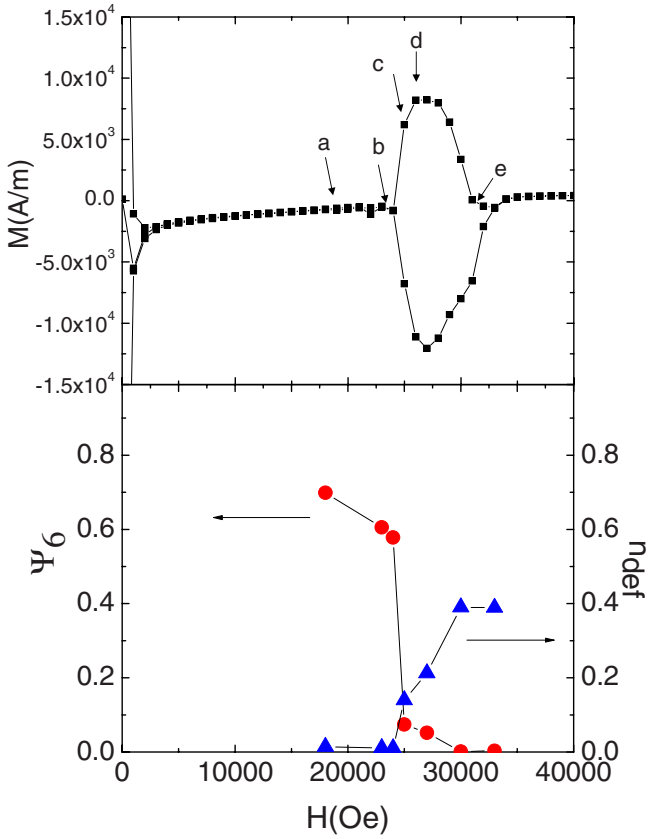

FIG. 5. (Color online) (a) Isothermal magnetization curves at 1.8 K for sample Co4 (T_c=5.7 K)—the same sample studied with STM. The arrows [(a)–(e)] indicate the values of applied magnetic fields at which STM images were acquired and they correspond to the values of fields in Figs. 4(a)–4(e), respectively. (b) Orientational order parameter Ψ_6 (circles) and coordination number n_{def} (triangles) as functions of the applied magnetic field, calculated from the STM images.

correlation image at the same field, the hexagonal order seems to be lost beyond the second-nearest neighbor. A similar situation is observed at H=2.7 T. At 3.3 T neither orientational order nor lattice periodicity is preserved.

From the Delauney triangulation of the STM images, it is possible to characterize the order-disorder transition by calculating two parameters: the normalized number of defects, n_{def}, in the VL, defined as the ratio between the number of vortices with a coordination number different from 6 and the total number of vortices; and the orientational order parameter Ψ_6, defined as $\Psi_6=\langle\exp(i6\theta)\rangle$, where θ is the bond orientation angle. In Fig. 5(b) both n_{def} and Ψ_6 are shown as functions of the applied magnetic field. The abrupt change in the orientational order parameter at 2.5 T suggests a possibility of a VL first-order phase transition. The mean-square displacement of the first-nearest neighbor calculated at a field just below this jump (H=2.4 T) is $\sqrt{\langle[u(a)-u(0)]^2\rangle}=0.12a_0$, where $a_0=1.07(\Phi_0/B)^{1/2}$ is the mean vortex spacing and Φ_0 is the flux quantum. This closely corresponds to the Lindemann melting criterion $\sqrt{\langle(u)^2\rangle}=c_L a_0$, with $c_L\approx 0.15-0.25$. However, it is worth noting that the finite size of the scanning area can also induce a jump in the orientational order parameter and it is difficult to make a definite conclusion about the phase-transition order.

V. ANALYSIS OF THE PEAK-EFFECT FEATURES

A. Pinning force due to fluctuation of local concentration of pair-breaking impurities

In the weak-collective-pinning scenario, only fluctuations in the defect density and therefore fluctuations in the local pinning force produce pinning. In the vicinity of the superconducting transition temperature, the pinning landscape is conveniently described by the Ginzburg-Landau theory's free-energy functional F (Ref. 25):

$$F=\int\left[\alpha|\Psi|^2+\frac{1}{2m}\left|\left(\frac{\hbar}{i}\frac{d}{dx_\mu}-\frac{2e}{c}A_\mu\right)\Psi\right|^2+\cdots\right]d^3\mathbf{r}, \tag{2}$$

with $\alpha=\alpha_0(T-T_c)$. Local variations in the critical temperature T_c due to the local fluctuation of defect density (T_c disorder) will affect the first term of the free energy as $\alpha\rightarrow\delta\alpha\propto\delta T_c$, while local variation in the mean free path l (mean-free-path disorder) will affect the second term of the free energy as $m\rightarrow\delta m\propto\delta l$. In the following we will consider only the effect of T_c disorder due to local fluctuation of impurity concentration. The local critical temperature T_c defined in the correlation volume $V_c\sim\pi\xi_{ab}^2\xi_c$ is given by the expression

$$T_c(\mathbf{r})=T_c(n)+\frac{dT_c}{dn}\frac{\delta N(\mathbf{r})}{V_c}, \tag{3}$$

where n is the average defect density and $\delta N(\mathbf{r})$ is the fluctuation of number of defects in the correlation volume near $\mathbf{r}$. The fluctuations in the impurity number in the volume V_c given by $\langle(\delta N)^2\rangle\approx$N corresponds to the fluctuation of T_c:

$$\langle[\delta T_c(\mathbf{r})]^2\rangle=\left(\frac{dT_c}{dn}\right)^2\frac{n}{V_c}. \tag{4}$$

The fluctuations in local T_c will cause a random local force on the VL per unit volume V_c. The random term in the Ginzburg-Landau free energy is

$$\delta E=\int\alpha_0\delta T_c(\mathbf{r})|\Psi(\mathbf{r}-\mathbf{u})|^2d^3\mathbf{r}. \tag{5}$$

The correlation function of the pinning force acting on the volume V of the vortex lattice is given by

$$\begin{aligned}\langle F_\nu(\mathbf{u})F_\mu(\mathbf{u}')\rangle&=VWf_F\left(\frac{\mathbf{u}-\mathbf{u}'}{\xi_{ab}}\right)\delta_{\nu\mu}\\&=\int_V\int_V\alpha_0^2\langle\delta T_c(\mathbf{r})\delta T_c(\mathbf{r}')\rangle\\&\quad\times\frac{|\partial\Psi(\mathbf{r}-\mathbf{u})|^2}{\partial u_\nu}\frac{|\partial\Psi(\mathbf{r}'-\mathbf{u}')|^2}{\partial u_\mu}d^3\mathbf{r}d^3\mathbf{r},\end{aligned} \tag{6}$$

where $f_F(\mathbf{v})$ is dimensionless function normalized as $f_F(0)$

=1. The bulk pinning force on VL is determined by the pinning strength W, via $F_{\text{pin}}=J_cB=\sqrt{W/V_c}$. Using Eqs. (4) and (6), we derive

$$W=\alpha_0^2(dT_c/dn)^2n\langle[\partial|\psi(\mathbf{r})|^2/\partial r_\nu]^2\rangle_{\mathbf{r}}$$
$$\approx n\left(\frac{dT_c}{dn}\right)^2\frac{B}{\Phi_0}(1-b)^2\left[\frac{H_c^2}{4\pi(T_c-T)}\right]^2.$$

Here we used the relations $\langle[\partial|\psi(\mathbf{r})|^2/\partial r_\nu]^2\rangle_{\mathbf{r}} \approx (B/\Phi_0)\langle|\psi_0^2|\rangle^2$ and $\alpha_0\langle|\psi_0^2|\rangle\approx H_c^2(1-b)/[4\pi(T_c-T)]$, where $H_c\propto T_c-T$ is the thermodynamic critical field, and $b=B/B_{c2}$ is the reduced magnetic field. Separating field dependence $W=W_0b(1-b)^2$, we rewrite W_0 as

$$W_0\approx n\left(\frac{dT_c/dn}{T_c}\right)^2\left(\frac{H_{c2}}{\Phi_0}\right)^3\varepsilon_0^2, \tag{7}$$

where $\varepsilon_0=\Phi_0^2/(4\pi\lambda_{ab})^2$, λ_{ab} is the in-plane London penetration depth, n is the density of pinning centers per unit volume, and dT_c/dn is the rate of decrease in the superconducting critical temperature as a function of density of pinning centers. Although, strictly speaking, this result is valid only in the Ginzburg-Landau region near the transition temperature, we expect that it can be used as an estimate at all temperatures.

B. Estimates of critical current density

The samples doped with Co correspond to the situation of pinning by large number of weak pinning centers described by the Larkin-Ovchinnikov theory.[6] This theory predicts several pinning regimes. At magnetic fields significantly smaller than the upper critical field, collective pinning of well-ordered vortex lattice is expected and the theory predicts exponentially small critical current. This regime corresponds to the region below the J_c peak where the value of the critical current is below our experimental resolution. The region of the peak effect where the vortex lattice is destroyed corresponds to the intermediate regime, and the Larkin-Ovchinnikov theory does not provide reliable quantitative prediction for the critical current. Another simple regime appears above the J_c peak, close to H_{c2}, where the vortex lines are pinned independently. In this single-vortex-pinning regime, the theory predicts that the critical current density vanishes as $J_c\propto(H_{c2}-B)$ with

$$\frac{dJ_c}{dB}\approx\frac{1.9}{H_{c2}\Phi_0}\left[\frac{\gamma^2W_0^2\lambda_{ab}^2}{H_{c2}^2\xi}\right]^{1/3}. \tag{8}$$

By introducing the experimental values of T_c, n, dT_c/dn, H_{c2}, ξ, and the anisotropy of the upper critical field γ, we can compare the theoretical estimate and the experimental slopes of the critical current density in the high-field region. In Fig. 6 the experimental values of dJ_c/dB for samples with different Co concentrations are compared with the theoretical estimates obtained by Eq. (8). It is worth noting that the theoretical estimates were obtained using experimental values for specific parameters in Eq. (8) corresponding to particular samples and that no fitting parameters were used. Therefore, we find good qualitative agreement for $\frac{dJ_c}{dB}$ in spite of the fact

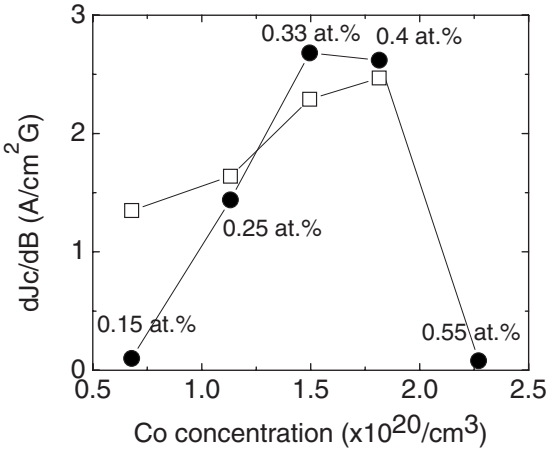

FIG. 6. The experimental slopes dJ_c/dB at 1.8 K above the peak-effect region (circles) for different Co concentrations together with the theoretical estimates (squares) derived from the Larkin-Ovchinnikov description of the critical current density.

that the onset of the peak effect is not in agreement with Larkin-Ovchinnikov theory. Also, it seems that the theoretical model cannot reproduce the nonmonotonic behavior of the slope in the critical current density. On the other hand, it is clear that at high defect density the same relation cannot hold since a more homogeneous landscape of pinning centers is less effective in pinning the VL.

In the case of Mn_xNbSe_2 the calculation of the field-independent part of the pinning strength from Eq. (7) leads to a value of W_0/n almost 20 times higher than the one obtained for Co_xNbSe_2. The origin of this discrepancy could be found in the much higher rate of decrease in the superconducting critical temperature T_c with Mn concentration. Indeed, the number of Mn ions per correlation volume V_c is limited to just a few. Therefore, the presence of a peak effect of comparable size to the one obtained with a much higher defect density of Co atoms points toward an increased pair-breaking strength of Mn.

In conclusion, we studied the evolution of the peak effect in Co_xNbSe_2 and Mn_xNbSe_2 single crystals as a function of Co and Mn atomic impurity concentration. We correlated the structure of the VL, studied by low-temperature STM, with the peak effect in critical current density measured by dc magnetization. First, we found an abrupt change in the orientational order parameter and in the number of defects in the VL at a magnetic field corresponding to the peak-effect regime, signifying a possible first-order phase transition in VL. At the same magnetic field we also found a sudden change in the VL nearest-neighbor mean-square displacement closely corresponding to the Lindemann melting criterion. Second, a doping dependence study revealed that a wide region of reversible magnetization that extends to very low applied magnetic fields (in the case of Co doping) can be attributed to a decrease in the anisotropy of the upper critical field. In the case of Co intercalates, the slope of the critical current density close to H_{c2} can be explained in the framework of Larkin-Ovchinnikov theory, with the pinning caused by local variations in superconducting critical temperature T_c. However, the field of the peak-effect onset does not

change with doping and this is not in line with the Larkin-Ovchinnikov theory. Contrary to the Co case, the Mn dopant acts as a strong pinning center for the VL as it has a higher localized magnetic moment and suppresses T_c much more effectively. In this case the number of pins in the correlation volume V_c is just small and therefore the peak effect cannot be described by the weak-collective-pinning formalism.

ACKNOWLEDGMENTS

The authors would like to thank V. Vinokur and A. Snezhko for useful discussions. They also would like to acknowledge the partial support by CNR under the short-term mobility program for researchers (R.D.C.) and the support by the International Frontier Center for Advanced Materials (IFCAM) at Tohoku University, Japan (M.I.). Financial support from NSF-DMR is acknowledged (M.G.K.). This work, as well as the use of the Center for Nanoscale Materials and the Electron Microscopy Center at Argonne National Laboratory, was supported by UChicago Argonne, LLC, operator of Argonne National Laboratory ("Argonne"). Argonne, a U.S. Department of Energy Office of Science laboratory, is operated under Contract No. DE-AC02-06CH11357.

*Present address: Center for Nanoscale Materials, Argonne National Laboratory, Argonne, Illinois 60439.

[1] M. A. R. Le Blanc and W. A. Little, Proceedings of the Seventh International Conference on Low-Temperature Physics (University of Toronto Press, Toronto, 1960), p. 198.
[2] K. Kadowaki and T. Mochiku, Physica C **195**, 127 (1992).
[3] L. A. Angurel, F. Amin, M. Polichetti, J. Aarts, and P. H. Kes, Phys. Rev. B **56**, 3425 (1997).
[4] P. H. Kes and C. C. Tsuei, Phys. Rev. Lett. **47**, 1930 (1981).
[5] S. S. Banerjee, N. G. Patil, S. Ramakrishnan, A. K. Grover, S. Bhattacharya, P. K. Mishra, G. Ravikumar, T. V. Chandrasekhar Rao, V. C. Sahni, M. J. Higgins, C. V. Tomy, G. Balakrishnan, and D. McK. Paul, Phys. Rev. B **59**, 6043 (1999).
[6] A. I. Larkin and Yu. N. Ovchinnikov, J. Low Temp. Phys. **34**, 409 (1979).
[7] A. Tonomura, H. Kasai, O. Kamimura, T. Matsuda, K. Harada, Y. Nakayama, J. Shimoyama, K. Kishio, T. Hanaguri, K. Kitazawa, M. Sasase, and S. Okayasu, Nature (London) **412**, 620 (2001).
[8] Y. Fasano, M. Menghini, F. de la Cruz, Y. Paltiel, Y. Myasoedov, E. Zeldov, M. J. Higgins, and S. Bhattacharya, Phys. Rev. B **66**, 020512 (2002).
[9] J. R. Kirtley, C. C. Tsuei, M. Rupp, J. Z. Sun, L. S. Yu-Jahnes, A. Gupta, M. B. Ketchen, K. A. Moler, and M. Bhushan, Phys. Rev. Lett. **76**, 1336 (1996).
[10] P. L. Gammel, U. Yaron, A. P. Ramirez, D. J. Bishop, A. M. Chang, R. Ruel, L. N. Pfeiffer, E. Bucher, G. D'Anna, D. A. Huse, K. Mortensen, M. R. Eskildsen, and P. H. Kes, Phys. Rev. Lett. **80**, 833 (1998).
[11] A. M. Troyanovski, M. van Hecke, N. Saha, J. Aarts, and P. H. Kes, Phys. Rev. Lett. **89**, 147006 (2002).
[12] A. R. Beal, *Physics and Chemistry of Materials with Layered Structures*, in Intercalated Layer Materials, edited by F. Lévy (D. Reidel, Dordrecht, 1979), p. 270.
[13] C. S. Oglesby, E. Bucher, C. Kloc, and H. Hohl, J. Cryst. Growth **137**, 289 (1994).
[14] J. J. Hauser, M. Robbins, and F. J. DiSalvo, Phys. Rev. B **8**, 1038 (1973).
[15] J. P. Gras, P. Haen, P. Monceau, G. Waysand, P. Molinie, and J. Rouxel, Nuovo Cimento B **38**, 519 (1977).
[16] S. S. P. Parkin and R. H. Friend, Philos. Mag. B **41**, 65 (1980).
[17] J. M. Voorhoeve-van Den Berg and R. C. Sherwood, J. Phys. Chem. Solids **32**, 167 (1971).
[18] C. P. Bean, Rev. Mod. Phys. **36**, 31 (1964).
[19] X. S. Ling, J. E. Berger, and D. E. Prober, Phys. Rev. B **57**, R3249 (1998).
[20] S. Foner and E. J. McNiff, Jr., Phys. Lett. **45A**, 429 (1973).
[21] N. Toyota, H. Nakatsuji, K. Noto, A. Hoshi, N. Kobayashi, Y. Muto, and Y. Onodera, J. Low Temp. Phys. **25**, 485 (1976).
[22] R. E. Schwall, G. R. Stewart, and T. H. Geballe, J. Low Temp. Phys. **22**, 557 (1976).
[23] A comprehensive review on the physics of vortices can be found in G. Blatter, M. V. Feigel'man, V. B. Geshkenbein, A. I. Larkin, and V. M. Vinokur, Rev. Mod. Phys. **66**, 1125 (1994), and references therein.
[24] F. F. Preparata and M. L. Shamos, *Computational Geometry: An Introduction* (Springer-Verlag, New York, 1985).
[25] V. L. Ginzburg and L. D. Landau, Zh. Eksp. Teor. Fiz. **20**, 1064 (1950).